

Hybrid protoneutron stars with the MIT bag model

O. E. Nicotra, M. Baldo, G. F. Burgio, and H.-J. Schulze
*Dipartimento di Fisica e Astronomia, Università di Catania and
INFN, Sezione di Catania, Via Santa Sofia 64, 95123 Catania, Italy*
(Dated: September 17, 2018)

We study the hadron-quark phase transition in the interior of protoneutron stars. For the hadronic sector, we use a microscopic equation of state involving nucleons and hyperons derived within the finite-temperature Brueckner-Bethe-Goldstone many-body theory, with realistic two-body and three-body forces. For the description of quark matter, we employ the MIT bag model both with a constant and a density-dependent bag parameter. We calculate the structure of protostars with the equation of state comprising both phases and find maximum masses below 1.6 solar masses. Metastable heavy hybrid protostars are not found.

PACS numbers: 26.60.+c, 21.65.+f, 97.60.Jd, 12.39.Ba

I. INTRODUCTION

It is generally believed that a neutron star (NS) is formed as a result of the gravitational collapse of a massive star ($M \gtrsim 8M_{\odot}$) in a type-II supernova [1, 2]. Just after the core bounce, a protoneutron star (PNS) is formed, a very hot and lepton-rich object, where neutrinos are temporarily trapped. The following evolution of the PNS is dominated by neutrino diffusion, which results first in deleptonization and subsequently in cooling. The star stabilizes at practically zero temperature, and no trapped neutrinos are left.

The dynamical transformation of a PNS into a NS could be strongly influenced by a phase transition in the central region of the star. Calculations of PNS structure, based on a microscopic nucleonic equation of state (EOS), indicate that for the heaviest PNS, close to the maximum mass (about two solar masses), the central particle density reaches values larger than $1/\text{fm}^3$. In this density range the nucleon cores (dimension ≈ 0.5 fm) start to touch each other, and it is likely that quark degrees of freedom will play a role.

In a previous article [3] we have studied static properties of PNS assuming that nucleons, hyperons, and leptons are present in stellar matter. Our calculations are based on the EOS derived within the Brueckner-Bethe-Goldstone (BBG) theory of nuclear matter, extended to finite temperature. We have found that for purely nucleonic stars, both thermal effects and neutrino trapping slightly soften the EOS, thus reducing the value of the maximum mass. If hyperons are included, neutrino trapping shifts their onset to larger baryon density, and instead stiffens the EOS. This could lead to metastability during the subsequent evolution of the PNS to the late neutrino-free stage.

In this work we extend the previous calculations, and take into account a possible hadron-quark phase transition. In fact, as in the case of cold NS, the addition of hyperons demands for the inclusion of quark degrees of freedom in order to obtain a maximum mass larger than the observational lower limit. For this purpose we use the BBG EOS for describing the hadronic phase and the MIT bag model at finite temperature for the quark matter (QM) phase. We employ both a constant and a density-dependent bag parameter B . We find that the presence of QM increases the value of the maximum mass of a PNS, and stabilizes it at about $1.5\text{--}1.6 M_{\odot}$, no matter the value of the temperature. In contrast to purely hyperonic stars, neutrino trapping in hybrid stars does not increase the maximum mass and does not allow metastable states.

The paper is organized as follows. In section II we review the determination of the baryonic EOS comprising nucleons and hyperons in the finite-temperature Brueckner-Hartree-Fock approach. Section III concerns the QM EOS according to the MIT bag model. In section IV we present the results regarding PNS structure combining the baryonic and QM EOS for beta-stable nuclear matter. Section V contains our conclusions.

II. BRUECKNER THEORY

A. EOS of nuclear matter at finite temperature

In the recent years, the BBG perturbative theory for nuclear matter has made much progress, since its convergence has been firmly established [4] and it has been extended in a fully microscopic and self-consistent way to the hyperonic sector [5, 6, 7]. Only few microscopic calculations of the nuclear EOS at finite temperature are so far available. The first semi-microscopic investigation of the finite-temperature EOS was performed in Ref. [8]. The results predict a Van der Waals behavior for symmetric nuclear matter, which leads to a liquid-gas phase transition with a critical temperature $T_C \approx 18\text{--}20$ MeV. Later, Brueckner calculations [9, 10] and chiral perturbation theory at finite temperature [11] confirmed these findings with very similar

values of T_C . The Van der Waals behavior was also found in the finite-temperature relativistic Dirac-Brueckner calculations of [12, 13], although at a lower temperature.

The formalism which is closest to the BBG expansion, and actually reduces to it in the zero-temperature limit, is the one formulated in [14]. In this approach the essential ingredient is the two-body scattering matrix K , which, along with the single-particle potential U , satisfies the self-consistent equations

$$\begin{aligned} \langle k_1 k_2 | K(W) | k_3 k_4 \rangle &= \langle k_1 k_2 | V | k_3 k_4 \rangle \\ &+ \text{Re} \sum_{k'_3 k'_4} \langle k_1 k_2 | V | k'_3 k'_4 \rangle \frac{[1 - n(k'_3)][1 - n(k'_4)]}{W - E_{k'_3} - E_{k'_4} + i\epsilon} \langle k'_3 k'_4 | K(W) | k_3 k_4 \rangle \end{aligned} \quad (1)$$

and

$$U(k_1) = \sum_{k_2} n(k_2) \langle k_1 k_2 | K(W) | k_1 k_2 \rangle_A, \quad (2)$$

where k_i generally denote momentum, spin, and isospin. Here V is the two-body interaction, and we choose the Argonne V_{18} nucleon-nucleon potential [15]. $W = E_{k_1} + E_{k_2}$ represents the starting energy, $E_k = k^2/2m + U(k)$ the single-particle energy, and $n(k)$ is a Fermi distribution. At $T = 0$ Eq. (1) coincides with the Brueckner equation for the K matrix at zero temperature.

For given nucleon densities and temperature, Eqs. (1) and (2) have to be solved self-consistently along with the equations for the densities, $\rho_i = \sum_k n_i(k)$, and the free energy density, which has the following simplified expression

$$f = \sum_{i=n,p} \left[\sum_k n_i(k) \left(\frac{k^2}{2m_i} + \frac{1}{2} U_i(k) \right) - T s_i \right], \quad (3)$$

where

$$s_i = - \sum_k \left(n_i(k) \ln n_i(k) + [1 - n_i(k)] \ln [1 - n_i(k)] \right) \quad (4)$$

is the entropy density for component i treated as a free gas with spectrum $E_i(k)$.

In deriving Eq. (3), we have introduced the so-called *Frozen Correlations Approximation*, i.e., the correlations at $T \neq 0$ are assumed to be essentially the same as at $T = 0$. This means that the single-particle potential $U_i(k)$ for the component i can be approximated by the one calculated at $T = 0$. This allows to save computational time and simplify the numerical procedure. It turns out that the assumed independence is valid to a good accuracy, at least for not too high temperature (see Ref. [10], Fig. 12). For a more extensive discussion of this topic, the reader is referred to Ref. [16], and references therein.

In our many-body approach, we have also introduced three-body forces (TBF) among nucleons, in order to reproduce correctly the nuclear matter saturation point $\rho_0 \approx 0.17 \text{ fm}^{-3}$, $E/A \approx -16 \text{ MeV}$ and obtain values of incompressibility and symmetry energy at saturation point compatible with those extracted from phenomenology [17]. Since a complete microscopic theory of TBF is not available yet, we have adopted the phenomenological Urbana model [18], which in the BBG approach is reduced to a density-dependent two-body force by averaging over the position of the third particle, assuming that the probability of having two particles at a given distance is modified according to the two-body correlation function [10, 19].

The fast rise of the nucleon chemical potentials with density in NS cores [20, 21] may trigger the appearance of strange baryonic species, i.e., hyperons. For this purpose we have extended the BBG approach in order to include the Σ^- and Λ hyperons in a fully self-consistent way [5, 6]. In our work we have used the Nijmegen soft-core nucleon-hyperon (NH) potentials NSC89 [22], and neglected the hyperon-hyperon (HH) interactions, since so far no reliable HH potentials are available. Recently also calculations with the NSC97 potentials were concluded [7], which do include extensions to the HH sector, but yield very similar results.

The presence of hyperons strongly softens the EOS, mainly due to the larger number of baryonic degrees of freedom. This EOS produces a maximum NS mass that lies slightly below the canonical value of $1.44 M_\odot$ [23], which could indicate the presence of non-baryonic (quark) matter in the interior of heavy NS [24, 25, 26]. However, the quantitative effects of more reliable NH and HH potentials as well as of hyperonic TBF need still to be explored in the future. For these reasons, we will in this article perform finite-temperature calculations in a much simpler way by using non-interacting hyperons. This approximation is well justified for the present work, because the hadron-quark phase transition occurs at very low density, where hyperons do not yet play a role.

In any case, our microscopic baryonic EOS turns out to be very soft and features very different characteristics in comparison to the often used relativistic mean field (RMF) models. In particular, the combination of a QM phase with a RMF model leads usually to a reduction of the maximum NS mass [21, 24], whereas in our approach the maximum mass increases due to the presence of QM, which is in fact required in order to cover the current observational values of NS masses. Also for PNS very different properties will arise, as we will see.

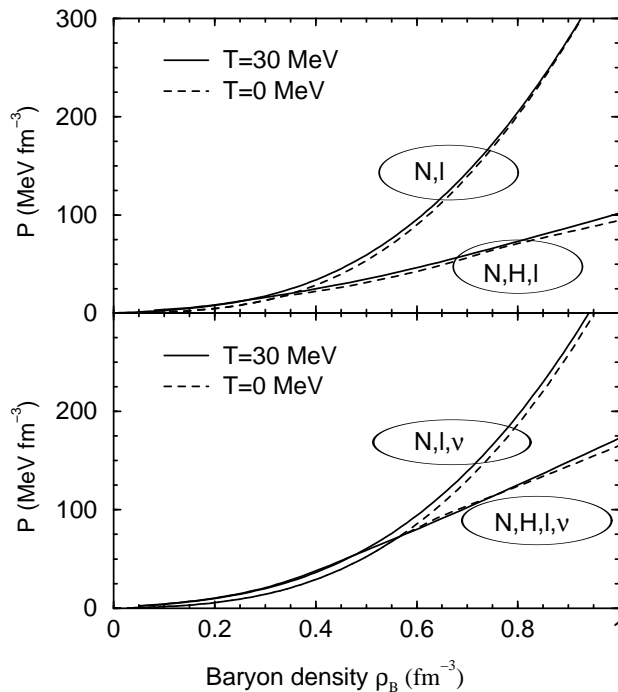


FIG. 1: The EOS in beta-stable baryon matter is displayed for temperatures $T = 0$ and 30 MeV. The upper (lower) panel displays results for neutrino-free (neutrino-trapped) matter, for purely nucleonic (upper curves) and hyperonic (lower curves) stellar matter.

B. Composition and EOS of hot stellar matter

For the determination of the composition of beta-stable baryonic matter, one needs to know the functional dependence of the free energy, Eq. (3), on the individual partial densities and on temperature. In Ref. [3] we have provided analytical parametrizations of our numerical results for this purpose. From the free energy density one can then calculate the nucleon chemical potentials

$$\mu_i = \frac{\partial f}{\partial \rho_i}, \quad (5)$$

whereas the chemical potentials of the noninteracting leptons and hyperons are obtained by solving numerically the free Fermi gas model at finite temperature.

For stars in which the strongly interacting particles are only baryons, the composition at given baryon density $\rho = \sum_i \rho_i$ is determined by the requirements of beta equilibrium and charge neutrality, i.e.,

$$\mu_i = b_i \mu_n - q_i (\mu_l - \mu_{\nu_l}), \quad (6)$$

$$0 = \sum_i q_i x_i + \sum_l q_l x_l, \quad (7)$$

where $x_i = \rho_i/\rho$ is the baryon concentration, b_i the baryon number, and q_i the electric charge of the species i . Equivalent quantities are defined for the leptons $l = e, \mu$. The initial PNS contains trapped neutrinos, so the electron and muon lepton numbers

$$Y_l = x_l - x_{\bar{l}} + x_{\nu_l} - x_{\bar{\nu}_l} \quad (8)$$

are conserved on dynamical time scales and we fix them to $Y_e = 0.4$ and $Y_\mu = 0$, as indicated by gravitational collapse calculations of the iron core of massive stars.

Solving these equations, we have found in [3] that the electron fraction is larger in neutrino-trapped than in neutrino-free matter, and, as a consequence, the proton population is larger. Moreover, neutrino trapping shifts the threshold density of the Σ^- to high density, whereas Λ 's appear at slightly smaller density. This is due to the fact that the Σ^- onset depends on the neutron and lepton chemical potentials, i.e., $\mu_{\Sigma^-} = \mu_n + \mu_e - \mu_{\nu_e}$, which stays at larger values in neutrino-trapped matter than in the neutrino-free case because of the larger fraction of electrons, thus delaying the appearance of the Σ^- to higher baryon

density and limiting its population to a few percent. On the other hand, the Λ onset depends on the neutron chemical potential only, $\mu_\Lambda = \mu_n$, which stays at slightly lower values in the neutrino-trapped case. When the temperature increases, the hyperon thresholds disappear and more and more hyperons are present also at low densities, but they represent only a small fraction of the total baryon density in this region of the PNS. Altogether, the hyperon fractions are much smaller than in the neutrino-free matter and therefore the corresponding EOS will be stiffer than in the neutrino-free case.

Once the composition of the beta-stable stellar matter is known, one can proceed to calculate the free energy density f and then the pressure p through the usual thermodynamical relation

$$p = \rho^2 \frac{\partial(f/\rho)}{\partial\rho}. \quad (9)$$

The resulting EOS is displayed in Fig. 1, where the pressure for beta-stable stellar matter, without (upper panel) and with (lower panel) neutrinos, is plotted as a function of the baryon density at temperatures $T = 0$ and 30 MeV. We notice that thermal effects produce a slightly stiffer EOS with respect to the cold case, and that at very high densities they almost play no role. The inclusion of hyperons, however, causes a dramatic effect, because the EOS gets much softer, no matter the value of the temperature. In the neutrino-trapped case, the EOS is slightly softer than in neutrino-free matter if only nucleons and leptons are present in the stellar matter. Also here the presence of hyperons introduces a strong softening of the EOS, but less than in the neutrino-free case, because now the hyperons appear later in the matter and their concentration is lower. This fact could lead to metastable stars which suffer a delayed collapse while cooling down, as discussed in [27].

III. QUARK MATTER EQUATION OF STATE

A. The MIT Bag Model

We review briefly the description of the bulk properties of uniform QM at finite temperature, deconfined from the beta-stable hadronic matter discussed in the previous section, by using the MIT bag model [28]. In its simplest form, the quarks are considered to be free inside a bag and the thermodynamic properties are derived from the Fermi gas model, where the quark $q = u, d, s$ baryon density, the energy density, and the free energy density are given by

$$\rho_q = \frac{g}{3} \int \frac{d^3k}{(2\pi)^3} [f_q^+(k) - f_q^-(k)], \quad (10)$$

$$\varepsilon_Q = g \sum_q \int \frac{d^3k}{(2\pi)^3} [f_q^+(k) + f_q^-(k)] E_q(k) + B, \quad (11)$$

$$f_Q = \varepsilon_Q - T \sum_q s_q, \quad (12)$$

where $g = 6$ is the quark degeneracy, $E_q(k) = \sqrt{m_q^2 + k^2}$, B is the bag constant, s_q the entropy density of a noninteracting quark gas, and the Fermi distribution functions for the quarks and anti-quarks are

$$f_q^\pm(k) = \frac{1}{1 + \exp[(E_q(k) \mp \mu_q)/T]} \quad (13)$$

with μ_q being the quark chemical potentials. The corresponding expressions at $T = 0$ can be obtained by eliminating the antiparticles and substituting the particle distribution functions by the usual step functions. We have used massless u and d quarks, and $m_s = 150$ MeV.

It has been found [24, 29] that within the MIT bag model (without color superconductivity) with a density-independent bag constant B , the maximum mass of a NS cannot exceed a value of about 1.6 solar masses. Indeed, the maximum mass increases as the value of B decreases, but too small values of B are incompatible with a hadron-quark transition density $\rho > 2-3 \rho_0$ in nearly symmetric nuclear matter, as demanded by heavy-ion collision phenomenology. Values of $B \gtrsim 150$ MeV/fm⁻³ can also be excluded within our model, since we do not obtain any more a phase transition in beta-stable matter in combination with our baryonic EOS [24].

In order to overcome these restrictions of the model, one can introduce a density-dependent bag parameter $B(\rho)$, and this approach was followed in Ref. [24]. This allows one to lower the value of B at large density, providing a stiffer QM EOS and increasing the value of the maximum mass, while at the same time still fulfilling the condition of no phase transition below $\rho \approx 3\rho_0$ in symmetric matter. In the following we present results based on the MIT model using both a constant value of the bag parameter, $B = 90$ MeV/fm³, and a gaussian parametrization for the density dependence,

$$B(\rho) = B_\infty + (B_0 - B_\infty) \exp\left[-\beta \left(\frac{\rho}{\rho_0}\right)^2\right] \quad (14)$$

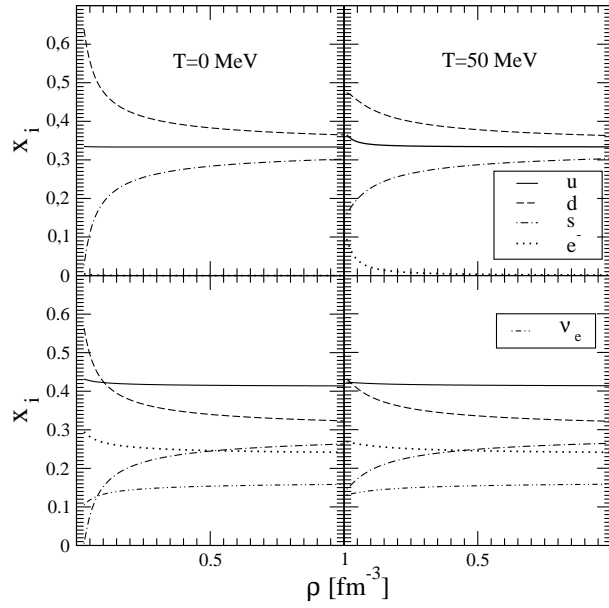


FIG. 2: Particle fractions in beta-stable QM at $T = 0$ (left panels) and $T = 50$ MeV (right panels) for neutrino-free (upper panels) and neutrino-trapped (lower panels) matter.

with $B_\infty = 50 \text{ MeV}/\text{fm}^{-3}$, $B_0 = 400 \text{ MeV}/\text{fm}^3$, and $\beta = 0.17$, see Ref. [24].

The introduction of a density-dependent bag has to be taken into account properly for the computation of various thermodynamical quantities; in particular the quark chemical potentials and the pressure are modified as

$$\mu_q \rightarrow \mu_q + \frac{dB(\rho)}{d\rho}, \quad (15)$$

$$p \rightarrow p + \rho \frac{dB(\rho)}{d\rho}. \quad (16)$$

Nevertheless, due to a cancelation of the second term in (15), occurring in relations (17) for the beta-equilibrium, the composition at a given total baryon density remains unaffected by this term (and is in fact independent of B). At this stage of investigation, we disregard possible dependencies of the bag parameter on temperature and individual quark densities. For a more extensive discussion of this topic, the reader is referred to Refs. [24, 25, 26].

B. Quark matter in beta equilibrium

In a PNS with QM and trapped neutrinos we must add the contribution of the leptons as free Fermi gases to the (free) energy density, Eqs. (11,12), and impose beta equilibrium, charge neutrality, and baryon and lepton number conservation [21].

More precisely, the individual quark chemical potentials are fixed by Eq. (6) with $b_q = 1/3$, which implies

$$\mu_d = \mu_s = \mu_u + \mu_l - \mu_{\nu_l}. \quad (17)$$

The charge neutrality condition and the total baryon number conservation read

$$0 = 2\rho_u - \rho_d - \rho_s - \rho_e, \quad (18)$$

$$\rho = \rho_u + \rho_d + \rho_s, \quad (19)$$

and Eq. (8) specifies lepton number conservation. These equations determine the composition $\rho_q(\rho)$ and the pressure of the QM phase,

$$p_Q(\rho) = \rho \frac{\partial f_Q}{\partial \rho} - f_Q. \quad (20)$$

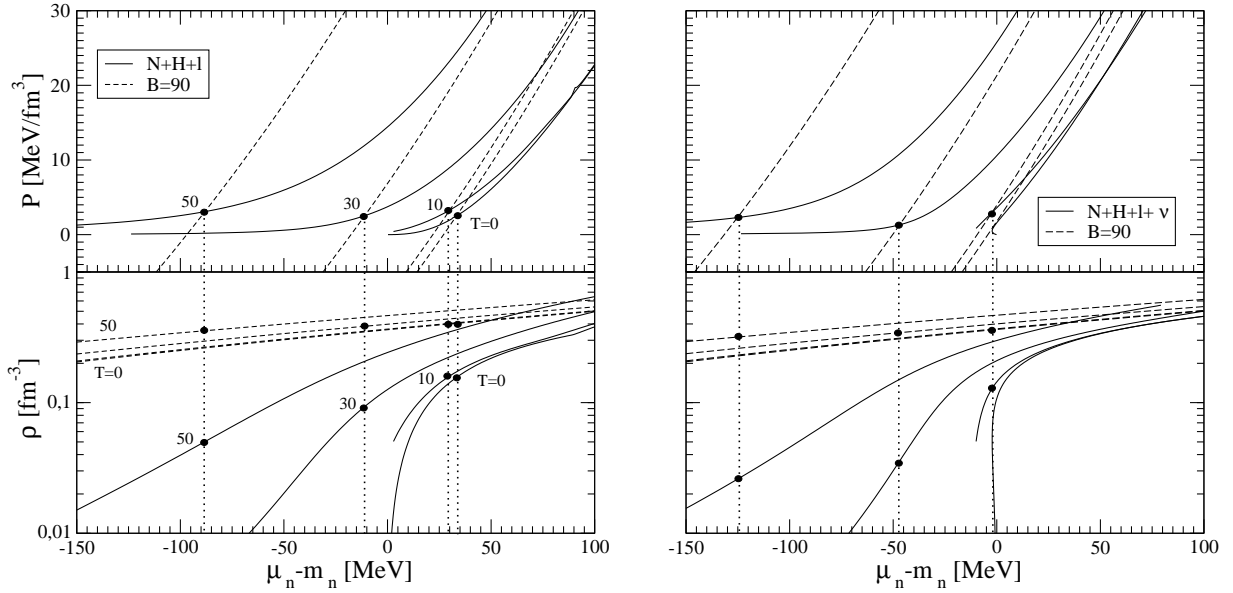


FIG. 3: Baryon density (lower panels) and pressure (upper panels) as a function of baryon chemical potential of beta-stable baryonic matter (solid curves) and quark matter (dashed curves) with (right panels) and without (left panels) neutrino trapping at different temperatures $T = 0, 10, 30, 50$ MeV. The vertical dotted lines indicate the positions of the phase transitions. A bag constant $B = 90$ MeV/fm³ is used for QM.

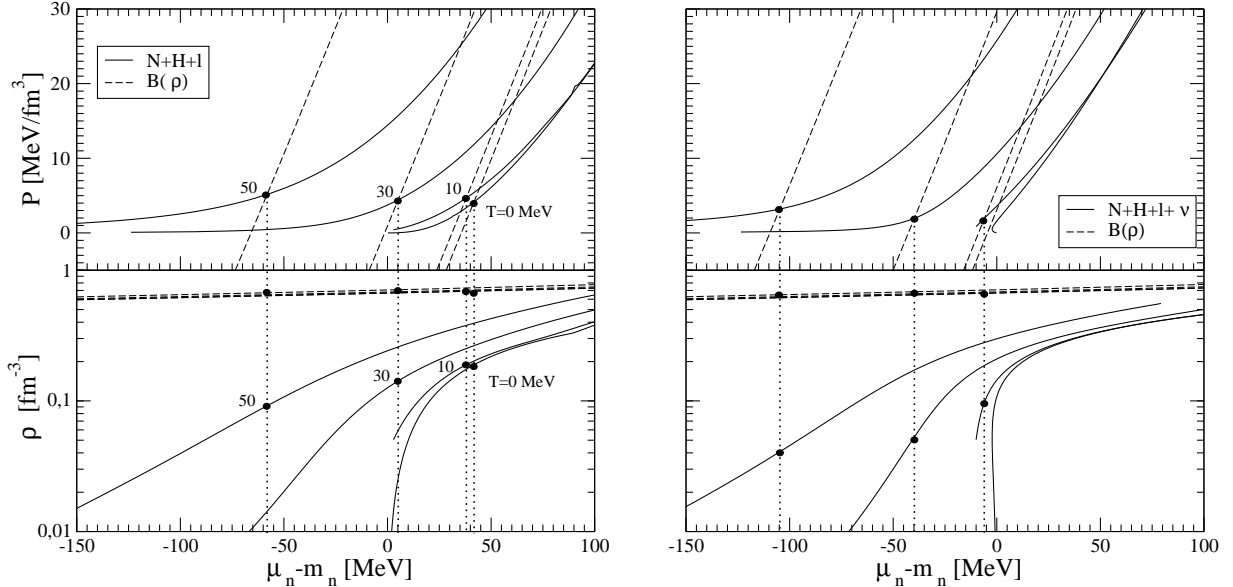


FIG. 4: Same as Fig. 3, but with a density-dependent bag parameter.

In Fig. 2 we plot the particle fractions $x_i = \rho_i/\rho$ as a function of baryon density for neutrino-free (upper panels) and neutrino-trapped (lower panels) QM. Since in the range of temperature considered here thermal effects are rather weak, we report only results for $T = 0$ and $T = 50$ MeV. Conversely, the presence of neutrinos influences quite strongly the composition: In this case the relative fraction of u quarks increases substantially from 33% to about 42%, compensating the charge of the electrons that are present at an average percentage of 25% throughout the considered range of baryon density, whereas d and s quark fractions are slightly lowered. One also can argue from the figure that most of the electrons present in the neutrino-free case come from thermally excited pairs.

Before studying the phase transition inside PNS, we would like to reiterate the fact that our combination of baryonic and

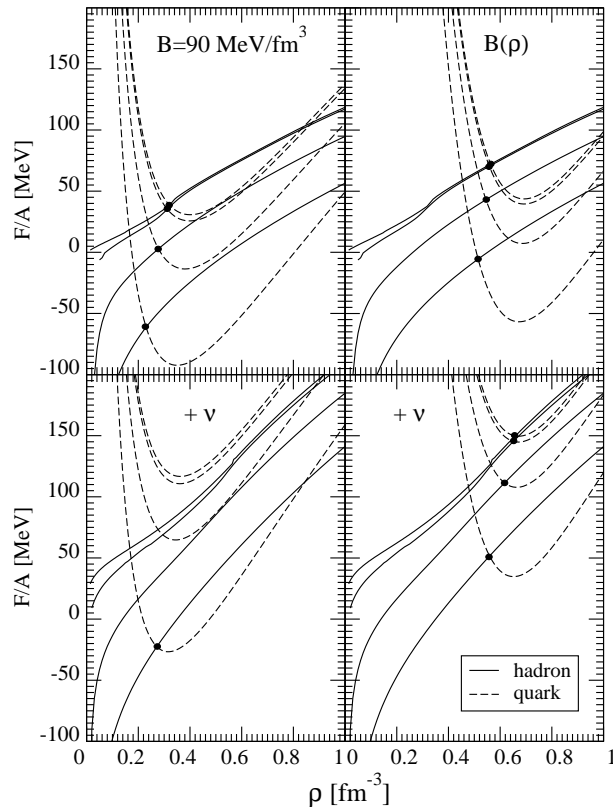


FIG. 5: Free energy per baryon as a function of baryon density of beta-stable baryonic matter (solid lines) and quark matter (dashed lines) with a bag constant $B = 90 \text{ MeV/fm}^3$ (left panels) or a density-dependent bag parameter (right panels) with (lower panels) and without (upper panels) neutrino trapping at different temperatures $T = 0, 10, 30, 50 \text{ MeV}$ (upper to lower curves).

QM EOS does not allow any phase transition in symmetric nuclear matter below about $3\text{--}4 \rho_0$, as ruled out by observational evidence. This has been amply discussed in Refs. [24, 25, 26] and was actually an important motivation for our choice of the QM EOS, as mentioned above.

C. Phase transition in hot beta-stable matter

We now consider the hadron-quark phase transition in beta-stable matter at finite temperature. In the present work we adopt the simple Maxwell construction for the phase transition from the plot of pressure versus chemical potential. The more general Glendenning (Gibbs) construction [21, 30] is still affected by many theoretical uncertainties [31] and in any case influences very little the final mass-radius relations of massive (proto)neutron stars [24].

We therefore display in Figs. 3 and 4 the pressure p (upper panels) and baryon density ρ (lower panels) as functions of the baryon chemical potential μ_B for both baryonic and QM phases at temperatures $T = 0, 10, 30, 50 \text{ MeV}$. The crossing points of the baryon and quark pressure curves (marked with a dot) represent the transitions between baryon and QM phases. The projections of these points (dotted lines) on the baryon and quark density curves in the lower panels indicate the corresponding transition densities from low-density baryonic matter, ρ_H , to high-density QM, ρ_Q . The results in Fig. 3 are obtained with $B = 90 \text{ MeV/fm}^3$ and those in Fig. 4 with $B(\rho)$.

The following general observations can be made:

- (i) The transition density ρ_H is rather low, of the order of the nuclear matter saturation density;
- (ii) The phase transition density jump $\rho_Q - \rho_H$ is large, several times ρ_H ;
- (iii) Thermal effects shift ρ_H to lower values of subnuclear densities and increase the density jump $\rho_Q - \rho_H$;
- (iv) Neutrino trapping lowers even more the transition density. For the cold case the presence of neutrinos even inhibits completely the phase transition. However, this feature has no physical relevance, because no trapping occurs in cold catalyzed neutron stars. The reason for such behavior is the stronger increase of the QM pressure due to neutrino trapping compared to the one of the baryonic phase, as evidenced in the figure. This leads naturally to an earlier onset of the QM phase;
- (v) The model with density-dependent bag parameter predicts (by construction, see the discussion above) larger transition den-

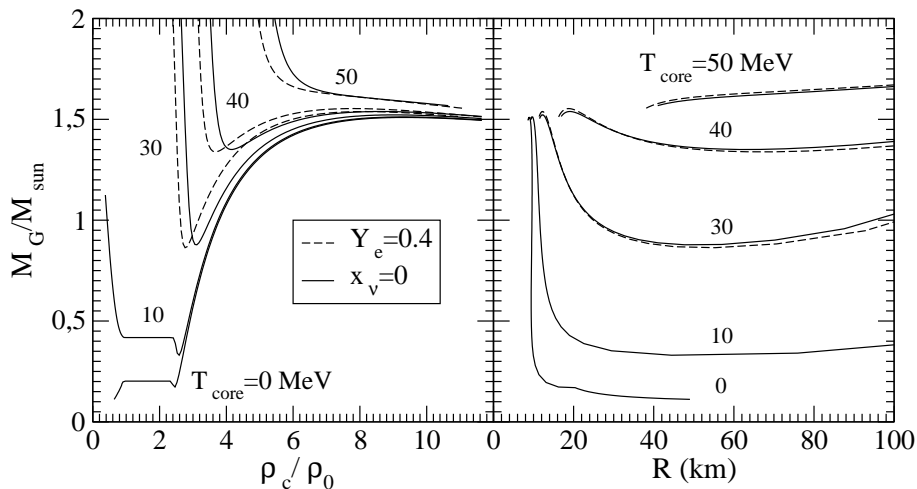


FIG. 6: (Proto)neutron star mass-central density (left panel) and mass-radius (right panel) relations for different core temperatures $T = 0, 10, 30, 40, 50$ MeV and neutrino-free (solid curves) or neutrino-trapped (dashed curves) matter. A bag constant $B = 90$ MeV/fm³ is used for QM.

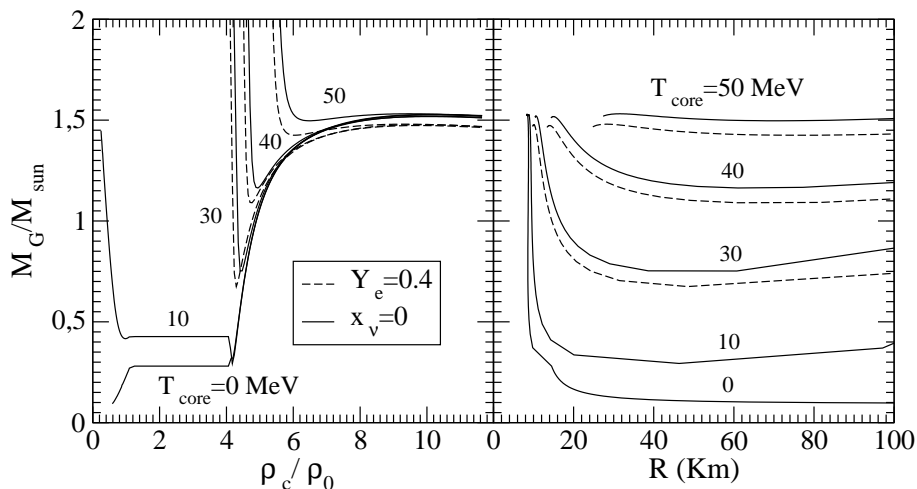


FIG. 7: Same as Fig. 6, but with a density-dependent bag parameter.

sities ρ_H and larger jumps $\rho_Q - \rho_H$ than those with bag constant $B = 90$ MeV/fm³. The plateaus in the Maxwell construction are thus wider for the former case.

These qualitative conclusions are reaffirmed in Fig. 5, where we report the free energy per baryon, F/A , as a function of baryon density, the four panels corresponding to the cases mentioned above with and without neutrino trapping and with different bag parameters. Here the crossing points between solid lines (baryon phase) and dashed lines (QM phase) indicate an average phase transition density, above which the QM phase is characterized by a value of the free energy lower than that of the baryon phase, thus indicating that the QM phase is energetically favoured.

Based on these results for the beta-stable baryon and QM phases, we proceed now to the determination of the properties of static (proto)neutron stars.

IV. PROTONEUTRON STAR STRUCTURE

We assume that a (proto)neutron star is a spherically symmetric distribution of mass in hydrostatic equilibrium. The equilibrium configurations are obtained by solving the Tolman-Oppenheimer-Volkoff (TOV) equations [1] for the pressure p and the

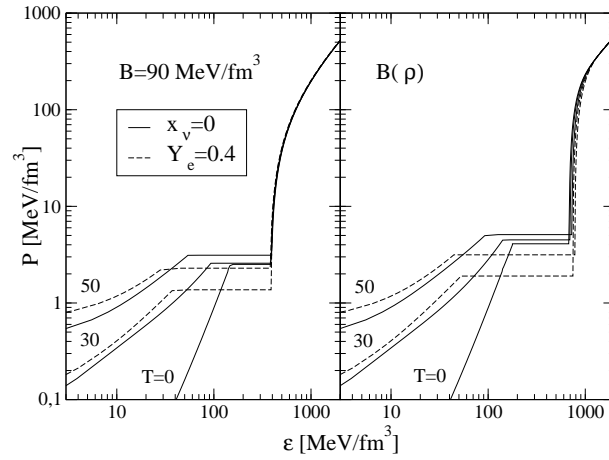


FIG. 8: Pressure as a function of energy density for beta-stable matter with (dashed curves) and without (solid curves) neutrino trapping at different temperatures $T = 0, 30,$ and 50 MeV with a bag constant $B = 90$ MeV/fm³ (left panel) or a density-dependent bag parameter (right panel).

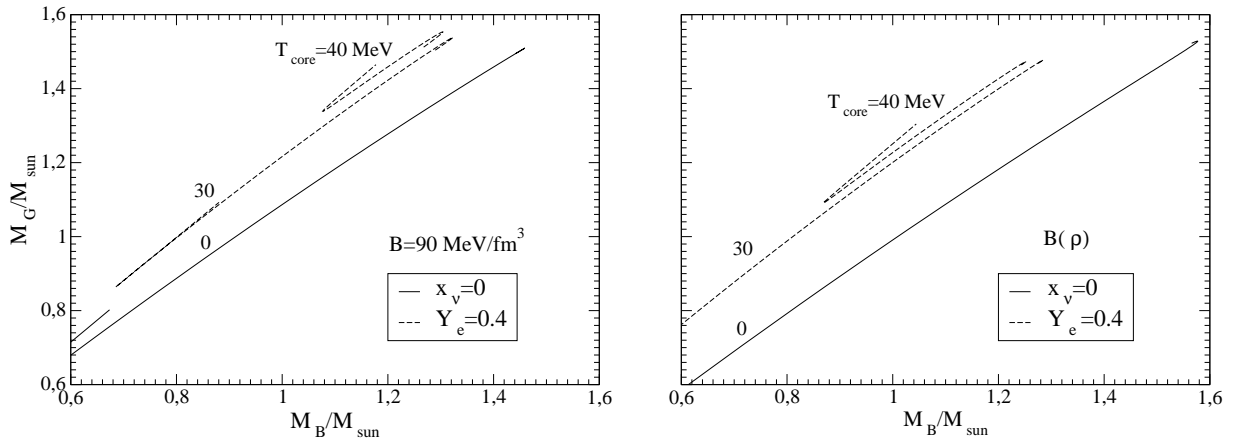


FIG. 9: Relation between gravitational mass and baryonic mass for cold neutron stars (solid curves) and protoneutron stars at $T = 30, 40$ MeV (dashed lines) with a bag constant $B = 90$ MeV/fm³ (upper panel) or a density-dependent bag parameter (lower panel).

enclosed gravitational mass m and baryonic mass m_B ,

$$\frac{dp(r)}{dr} = -\frac{Gm(r)\epsilon(r)}{r^2} \times \frac{[1 + p(r)/\epsilon(r)][1 + 4\pi r^3 p(r)/m(r)]}{1 - 2Gm(r)/r}, \quad (21)$$

$$\frac{dm(r)}{dr} = 4\pi r^2 \epsilon(r), \quad (22)$$

$$\frac{dm_B(r)}{dr} = \frac{4\pi r^2 \rho(r) m_N}{\sqrt{1 - 2Gm(r)/r}}, \quad (23)$$

where $m_N = 1.67 \times 10^{-24}$ g is the nucleon mass and G the gravitational constant. Starting with a central mass density $\epsilon(r=0) \equiv \epsilon_c$, we integrate out until the pressure on the surface equals the one corresponding to the density of iron. This gives the stellar radius R and the gravitational mass $M_G \equiv m(R)$ and baryonic mass $M_B \equiv m_B(R)$.

Moreover, in our model we assume that a PNS, in its early stage, is composed of a hot isothermal and neutrino-opaque core separated from an outer cold crust (described by the Baym-Pethick-Sutherland [32] and the Feynman-Metropolis-Teller [33] EOS) by an isentropic, beta-equilibrated, and neutrino-free intermediate layer in the range of baryon density from 0.01 fm⁻³ down to 10^{-6} fm⁻³ [34], which is based on the EOS LS220 of Lattimer and Swesty [35] with compressibility $K = 220$ MeV.

For the isothermal core we use as input the BHF EOS for the baryonic matter and the MIT bag models for the beta-stable QM phase, as discussed above. In order to ensure an exact matching of all the thermodynamic quantities between core and crust we perform a fine tuning of the entropy per baryon of the isentropic envelope, $S_{\text{env.}}$, around the matching value of baryon density $\rho_{\text{env.}} \approx 0.01 \text{ fm}^{-3}$. More precisely, fixing $S_{\text{env.}}$ to the values 6, 8, 10 (in units of the Boltzmann constant) we get temperature profiles which drop quickly from $T_{\text{core}} = 30, 40, 50 \text{ MeV}$ to zero in the considered range of density, thus suggesting a natural correspondence between values of T_{core} and $S_{\text{env.}}$ [34].

In other words, we model the PNS by adopting a hybrid isothermal plus isentropic temperature profile, allowing us to take into account as much as possible information coming from dynamical simulations [27, 36, 37, 38], which show that the temperature drops rapidly to zero at the surface of the star due to the fast cooling of the outer part of the PNS, where the stellar matter is transparent to neutrinos. In addition, during the early stage, the outer part of a PNS is characterized by a high value of the entropy per baryon. Essentially, in the first ten seconds, the entropy profile decreases from the surface to the core starting from values of 6–10 [36].

We consider this approach more realistic than the one employed for baryonic stars in [3], where a temperature profile in the shape of a step function was assumed, joining directly the baryonic EOS and the one for the cold outer crust. This procedure leads, however, to unstable PNS at T_{core} slightly above 30 MeV and also yields a strong dependence on the value of density where the cold crust is attached of the minimum PNS mass, which is a fundamental quantity characterizing the range of stability of such hot and compact objects. The improved procedure described above applied to baryonic PNS leads to more reliable values of the minimum gravitational mass, while hardly affecting the value of the maximum mass, which mainly depends on the EOS employed and the core composition. For the purely nucleonic case (no hyperons) we find now a maximum mass within a narrow range of 1.77–1.87 M_{\odot} [34], similar to [3].

In the following we present results schematizing the entire evolution of the star as divided in two main stages. The first consists of a PNS with a hot ($T_{\text{core}} \approx 30\text{--}50\text{MeV}$) neutrino-trapped core and a high-entropy transition layer ($S_{\text{env.}} \approx 6\text{--}10$), joined to a cold outer crust. The second stage represents the short-term cooling, where the neutrino-free core possesses a low temperature of about 10 MeV and is directly attached to a cold crust at $\rho = 3 \times 10^{-4} \text{ fm}^{-3}$.

A. Numerical Results

The results are plotted in Figs. 6 and 7, where we display the gravitational mass M_G (in units of the solar mass M_{\odot}) as a function of the radius R (right panels) and the central baryon density ρ_c (left panels), for QM EOS with $B = 90 \text{ MeV}/\text{fm}^3$ and $B(\rho)$, respectively.

Due to the use of the Maxwell construction, the curves are not continuous [21]: For small enough central densities (large radii) the stars are purely baryonic. Then a sudden increase of the central density is required in order to initiate the QM phase in the center of the star, corresponding to the phase diagrams Figs. 3 and 4. By performing the Glendenning construction, the curves would become continuous. Heavy PNS in our approach are thus practically quark stars with only a thin outer layer of baryonic matter. Below the maximum mass configuration, however, the stars develop an extended outer envelope of hot matter, the details of which depend on the treatment of the low-density baryonic phase and the phase transition. We will therefore in the following focus on the properties of heavy stars close to the limiting mass, which are unaffected by these complications.

For completeness we display the complete set of results at core temperatures $T = 0, 10, 30, 40, 50 \text{ MeV}$ with and without neutrino trapping, although only the curves with high temperatures and neutrino trapping and low temperatures without trapping are the physically relevant ones. We observe in any case a surprising insensitivity of the results to the presence of neutrinos, in particular for the $B = 90 \text{ MeV}/\text{fm}^3$ case, which can be traced back to the fact that the QM EOS $p(\varepsilon)$ is practically insensitive to the neutrino fraction. In fact, for the $B = 90 \text{ MeV}/\text{fm}^3$ case and assuming massless quarks and leptons, the universal relation $p = (\varepsilon - 4B)/3$ would hold irrespective of the internal composition of the quark-lepton phase. This is illustrated in Fig. 8, showing the beta-stable EOS $p(\varepsilon)$ at three temperatures with and without neutrinos. Indeed the pressure in the QM phase is nearly the same in both cases, even to a lesser degree for the $B(\rho)$ EOS.

On the other hand, the temperature dependence of the curves is quite pronounced for intermediate and low-mass stars, showing a strong increase of the minimum mass with temperature, whereas the maximum mass remains practically constant under all possible circumstances. Above core temperatures of about 40–50 MeV all stellar configurations become unstable.

Concerning the dependence on the QM EOS, we observe again only a slight variation of the maximum PNS masses between 1.55 M_{\odot} for $B = 90 \text{ MeV}/\text{fm}^3$ and 1.48 M_{\odot} for $B(\rho)$. Clearer differences exist for the radii, which for the same mass and temperature are larger for the $B = 90 \text{ MeV}/\text{fm}^3$ model, as has also been found in [24, 26] for cold NS. The maximum PNS masses turn out to be very close to those of cold NS, thus excluding the possibility of metastable configurations.

In order to illustrate better this issue, we show in Fig. 9 the relation between baryonic and gravitational mass for cold NS and PNS at $T = 30$ and 40 MeV. In this plot the evolution of an isolated star proceeds on vertical lines connecting the upper curve for PNS with the lower curve for NS. One notes immediately that metastable hybrid stars do not exist in our model: For the $B(\rho)$ case, the heaviest PNS ($M_B = 1.28M_{\odot}$, $M_G = 1.48M_{\odot}$) transits into a $M_G = 1.26M_{\odot}$ NS, which is consequently the heaviest

NS that can be produced without accretion in our approach. Accretion might then further augment the NS mass to a maximum stable value of $M_G = 1.53M_\odot$.

V. CONCLUSIONS

In this article we extended our previous works on cold baryonic [6] and hybrid [24, 25, 26] NS and baryonic PNS [3] to the case of hybrid PNS. We combined the most recent microscopic baryonic EOS in the BHF approach involving nuclear three-body forces and hyperons with two versions of a generalized MIT bag model describing the QM phase: One using a fixed bag constant, the other one a density-dependent bag parameter $B(\rho)$ in order to explore the maximum PNS mass that can be reached in this approach.

We modelled the profile of a PNS in an extremely simplified way with a constant lepton fraction $Y_e = 0.4$ and constant temperature of the core and an isentropic cover, leaving the core temperature as a global parameter. A really satisfying treatment would require coupled dynamical simulations for the various microscopic and macroscopic evolution equations, which is currently beyond our reach.

We found in Ref. [3] that purely baryonic (hyperonic) PNS can reach masses of about $1.5 M_\odot$, and nearly the same mass limit is now obtained also for hybrid PNS. The difference between both configurations lies in the transition to a cold NS, which for baryonic stars could lead to a delayed collapse to a black hole, as the cold baryonic NS cannot support masses up to $1.5 M_\odot$ [6], whereas this phenomenon is excluded for hybrid NS, which can sustain masses up to those of the PNS.

This result is in contrast to Ref. [39], where such metastability was found also for hybrid stars; however, with a much stiffer baryonic EOS and correspondingly larger value of the bag constant $B = 200 \text{ MeV/fm}^3$, which is excluded in our model. As mentioned before, our baryonic EOS is especially soft due to the presence of hyperons, compensating the repulsive character of nucleonic TBF at high density. Its associated maximum NS mass remains below 1.4 solar masses, and the presence of QM inside the star is *required* in order to reach larger maximum masses. We have thus shown that the presumed increase of the hadron-quark phase transition density due to the presence of neutrino trapping [39, 40, 41] is not a general feature, but might be reversed in combination with a very soft baryonic EOS.

Altogether, we once again confirm our prediction of rather low limiting masses for (proto)neutron stars, irrespective of variations of the baryonic or QM EOS. Therefore, the experimental observation of a very heavy ($M \gtrsim 1.8M_\odot$) NS, as claimed recently by some groups [42] ($M \approx 2.2M_\odot$), if confirmed, could hint to serious problems for the current rather simple theoretical modelling of the high-density quark matter phase, the assumptions about the phase transition between baryon and QM phase, or even for the TOV equations at extreme baryon densities.

-
- [1] S. L. Shapiro and S. A. Teukolsky, *Black Holes, White Dwarfs, and Neutron Stars* (John Wiley and Sons, New York, 1983).
 - [2] H. A. Bethe, Rev. Mod. Phys. **62**, 801 (1990).
 - [3] O. E. Nicotra, M. Baldo, G. F. Burgio, and H. J. Schulze, Astron. Astrophys. **451**, 213 (2006).
 - [4] B. D. Day, Phys. Rev. **C24**, 1203 (1981); H. Q. Song, M. Baldo, G. Giansiracusa, and U. Lombardo, Phys. Rev. Lett. **81**, 1584 (1998); M. Baldo, G. Giansiracusa, U. Lombardo, and H. Q. Song, Phys. Lett. **B473**, 1 (2000); M. Baldo, A. Fiasconaro, H. Q. Song, G. Giansiracusa, and U. Lombardo, Phys. Rev. **C65**, 017303 (2002); R. Sartor, Phys. Rev. **C73**, 034307 (2006).
 - [5] H.-J. Schulze, A. Lejeune, J. Cugnon, M. Baldo, and U. Lombardo, Phys. Lett. **B355**, 21 (1995); H.-J. Schulze, M. Baldo, U. Lombardo, J. Cugnon, and A. Lejeune, Phys. Rev. **C57**, 704 (1998).
 - [6] M. Baldo, G. F. Burgio, and H.-J. Schulze, Phys. Rev. **C58**, 3688 (1998); Phys. Rev. **C61**, 055801 (2000).
 - [7] H.-J. Schulze, A. Polls, A. Ramos, and I. Vidaña, Phys. Rev. **C73**, 058801 (2006).
 - [8] B. Friedman and V. R. Pandharipande, Nucl. Phys. **A361**, 502 (1981).
 - [9] A. Lejeune, P. Grangé, M. Martzloff, and J. Cugnon, Nucl. Phys. **A453**, 189 (1986).
 - [10] M. Baldo and L. S. Ferreira, Phys. Rev. **C59**, 682 (1999); M. Baldo, L. S. Ferreira, and O. E. Nicotra, Phys. Rev. **C69**, 034321 (2004).
 - [11] N. Kaiser, S. Fritsch, and W. Weise, Nucl. Phys. **A697**, 255 (2002).
 - [12] B. Ter Haar and R. Malfliet, Phys. Rev. Lett. **56**, 1237 (1986); Phys. Rep. **149**, 207 (1987).
 - [13] H. Huber, F. Weber, and M. K. Weigel, Phys. Rev. **C57**, 3484 (1999).
 - [14] C. Bloch and C. De Dominicis, Nucl. Phys., **7**, 459 (1958); **10**, 181,509 (1959).
 - [15] R. B. Wiringa, V. G. J. Stoks, and R. Schiavilla, Phys. Rev. **C51**, 38 (1995).
 - [16] M. Baldo, *Nuclear Methods and the Nuclear Equation of State*, (World Scientific, Singapore, 1999), International Review of Nuclear Physics, Vol. 8.
 - [17] W. D. Myers and W. J. Swiatecki, Nucl. Phys. **A601**, 141 (1996); Phys. Rev. **C57**, 3020 (1998).
 - [18] J. Carlson, V. R. Pandharipande, and R. B. Wiringa, Nucl. Phys. **A401**, 59 (1983); R. Schiavilla, V. R. Pandharipande, and R. B. Wiringa, Nucl. Phys. **A449**, 219 (1986).
 - [19] M. Baldo, I. Bombaci, and G. F. Burgio, Astron. Astrophys. **328**, 274 (1997); X. R. Zhou, G. F. Burgio, U. Lombardo, H.-J. Schulze, and W. Zuo, Phys. Rev. **C69**, 018801 (2004).

- [20] N. K. Glendenning, *Phys. Lett.* **B114**, 391 (1982); *Astrophys. J.* **293**, 470 (1985).
- [21] N. K. Glendenning, *Compact Stars, Nuclear Physics, Particle Physics, and General Relativity*, 2nd ed., 2000, Springer-Verlag, New York.
- [22] P. M. M. Maessen, Th. A. Rijken, and J. J. de Swart, *Phys. Rev.* **C40**, 2226 (1989).
- [23] R. A. Hulse and J. H. Taylor, *Astrophys. J.* **195**, L51 (1975); J. H. Taylor and J. M. Weisberg, *Astrophys. J.* **345**, 434 (1989).
- [24] G. F. Burgio, M. Baldo, P. K. Sahu, A. B. Santra, and H.-J. Schulze, *Phys. Lett.* **B526**, 19 (2002); G. F. Burgio, M. Baldo, P. K. Sahu, and H.-J. Schulze, *Phys. Rev.* **C66**, 025802 (2002).
- [25] M. Baldo, M. Buballa, G. F. Burgio, F. Neumann, M. Oertel, and H.-J. Schulze, *Phys. Lett.* **B562**, 153 (2003).
- [26] C. Maieron, M. Baldo, G. F. Burgio, and H.-J. Schulze, *Phys. Rev.* **D70**, 043010 (2004).
- [27] M. Prakash, I. Bombaci, M. Prakash, P. J. Ellis, J. M. Lattimer, and R. Knorren, *Phys. Rep.*, **280**, 1 (1997).
- [28] A. Chodos, R. L. Jaffe, K. Johnson, C. B. Thorn, and V. F. Weisskopf, *Phys. Rev.* **D9**, 3471 (1974).
- [29] M. Alford and S. Reddy, *Phys. Rev.* **D67**, 074024 (2003).
- [30] N. K. Glendenning, *Phys. Rev.* **D46**, 1274 (1992).
- [31] T. Endo, T. Maruyama, S. Chiba, and T. Tatsumi, *Prog. Theor. Phys.*, **115**, 337 (2006).
- [32] G. Baym, C. Pethick, and D. Sutherland, *Astrophys. J.* **170**, 299 (1971).
- [33] R. Feynman, F. Metropolis, and E. Teller, *Phys. Rev.* **C75**, 1561 (1949).
- [34] O. E. Nicotra, arXiv:nucl-th/0607055.
- [35] J. M. Lattimer and F. D. Swesty, *Nucl.Phys.* **A535**, 331 (1997).
- [36] A. Burrows and J. M. Lattimer, *Astrophys. J.* **307**, 178 (1986).
- [37] K. Strobel, C. Schaab, and M. K. Weigel, *Astron. Astrophys.* **350**, 497 (1999).
- [38] J. A. Pons, S. Reddy, M. Prakash, J. M. Lattimer, and J. A. Miralles, *Astrophys. J.* **513**, 780 (1999); L. Villain, J. A. Pons, P. Cerdá-Durán, and E.ourgoulhon, *Astron. Astrophys.* **418**, 283 (2004).
- [39] M. Prakash, J. R. Cooke, and J. M. Lattimer, *Phys. Rev.* **D52**, 661 (1995); A. W. Steiner, M. Prakash, and J. M. Lattimer, *Phys. Lett.* **B486**, 239 (2000); J. A. Pons, A. W. Steiner, M. Prakash, and J. M. Lattimer, *Phys. Rev. Lett.* **86**, 5223 (2001).
- [40] G. Lugones and O. G. Benvenuto, *Phys. Rev.* **D58**, 083001 (1998).
- [41] S. Epsztein Grynberg, M. C. Nemes, H. Rodrigues, M. Chiapparini, S. B. Duarte, A. H. Blin, and B. Hiller, *Phys. Rev.* **D62**, 123003 (2000).
- [42] P. Kaaret, E. Ford, and K. Chen, *Astrophys. J. Lett.* **480**, L27 (1997); W. Zhang, A. P. Smale, T. E. Strohmayer, and J. H. Swank, *Astrophys. J. Lett.* **500**, L171 (1998); D. J. Nice, E. M. Splaver, I. H. Stairs, O. Löhmer, A. Jessner, M. Kramer, and J. M. Cordes, *Astrophys. J.* **634**, 1242 (2005).